iRegNet: Non-Rigid Registration of MRI to Interventional US for Brain-Shift Compensation Using Convolutional Neural Networks

RAMY A. ZEINELDIN[ID]1,2,3, (Member, IEEE), MOHAMED E. KARAR[ID]3,4, (Member, IEEE), ZIAD ELSHAER[5], MARKUS SCHMIDHAMMER[5], JAN COBURGER[ID]5, CHRISTIAN R. WIRTZ[ID]5, OLIVER BURGERT[ID]2, AND FRANZISKA MATHIS-ULLRICH[ID]1

[1]Institute for Anthropomatics and Robotics, Karlsruhe Institute of Technology (KIT), 76131 Karlsruhe, Germany
[2]Research Group Computer Assisted Medicine (CaMed), Reutlingen University, 72762 Reutlingen, Germany
[3]Faculty of Electronic Engineering (FEE), Menoufia University, Minuf 32952, Egypt
[4]Department of Computer Engineering and Networks, College of Computing and Information Technology, Shaqra University, Riyadh 11961, Saudi Arabia
[5]Department of Neurosurgery, University of Ulm, Günzburg, 89312 Ulm, Germany

Corresponding author: Ramy A. Zeineldin (ramy.zeineldin@ieee.org)

ABSTRACT Accurate and safe neurosurgical intervention can be affected by intra-operative tissue deformation, known as brain-shift. In this study, we propose an automatic, fast, and accurate deformable method, called iRegNet, for registering pre-operative magnetic resonance images to intra-operative ultrasound volumes to compensate for brain-shift. iRegNet is a robust end-to-end deep learning approach for the non-linear registration of MRI-iUS images in the context of image-guided neurosurgery. Pre-operative MRI (as moving image) and iUS (as fixed image) are first appended to our convolutional neural network, after which a non-rigid transformation field is estimated. The MRI image is then transformed using the output displacement field to the iUS coordinate system. Extensive experiments have been conducted on two multi-location databases, which are the BITE and the RESECT. Quantitatively, iRegNet reduced the mean landmark errors from pre-registration value of (4.18 ± 1.84 and 5.35 ± 4.19 mm) to the lowest value of (1.47 ± 0.61 and 0.84 ± 0.16 mm) for the BITE and RESECT datasets, respectively. Additional qualitative validation of this study was conducted by two expert neurosurgeons through overlaying MRI-iUS pairs before and after the deformable registration. Experimental findings show that our proposed iRegNet is fast and achieves state-of-the-art accuracies outperforming state-of-the-art approaches. Furthermore, the proposed iRegNet can deliver competitive results, even in the case of non-trained images as proof of its generality and can therefore be valuable in intra-operative neurosurgical guidance.

INDEX TERMS Brain-Shift, computer-aided diagnosis, medical image registration, neurosurgery, intra-operative ultrasound.

I. INTRODUCTION

In neurosurgery, inferring the pathological tissue while avoiding damage to other surrounding anatomical structures is one of the key challenges. This is related to the difficulty of visually defining these pathologic structures from healthy tissue since most primary brain tumors grow by infiltration of healthy parenchyma [1]. Image-guided neurosurgery (IGN),

The associate editor coordinating the review of this manuscript and approving it for publication was Mauro Gaggero[ID].

the integration of medical imaging modalities with brain surgery has become an essential tool for assisting neurosurgeons to overcome the above challenge [2]. However, IGN systems have a major drawback since all these systems use pre-operative imaging on which the planning and interventional clinical phases are based. Neurosurgical manipulation, swelling due to osmotic drugs as well as anesthesia cause brain movements, known as "brain-shift", which dramatically limits the utility of pre-operative imaging for neurosurgical navigation [3]–[5].

Hence, IGN systems use a wide range of imaging modalities for measuring brain-shift in the operating room including intra-operative magnetic resonance images (iMRI) and intra-operative ultrasound images (iUS) [6]–[8]. In the case of iMRI, the brain displacement can be corrected by registering pre-operative MRI images with MRI images acquired during surgical procedures. Although iMRI offers soft-tissue contrast and diffusion-weighted imaging, it requires long scan times, may be associated with high costs, and the strong magnetic field can affect electronic systems. iUS is used as an alternative to iMRI providing inexpensive interventional imaging in real-time, however, with a reduced imaging quality compared with the iMRI. The use of three-dimensional reconstructed iUS is introduced in [9], allowing accurate and effective navigation.

Therefore, an automatic, fast, robust fusion of 3D-reconstructed iUS data with the pre-operative MRI images becomes highly important to accomplish the interventional procedures. However, the registration of misaligned pre-operative MRI images to the iUS is still a complex and challenging problem according to the type of information represented by each modality. Previous studies of medical image registration can be categorized into classical and learning-based methods [10]–[12]. Classical MRI to US image registration approaches include various choices of similarity metrics such as Correlation Coefficient (CC), and Correlation Ratio (CR), Mutual Information (MI), Normalized Correlation Coefficient (NCC), Self-Similarity Correlation (SSC), and Linear Correlation of Linear Combination (LC^2) [13]–[27]. One major drawback of the traditional methods is the high computational cost required to align every 3D MRI and iUS pair even with the efficient implementation on modern graphical processing units (GPUs).

Recently, deep learning, a subfield of artificial intelligence, has gained increasing popularity because of its outstanding performance in various computer vision and image analysis applications including, but not limited to object detection [28], feature extraction [29], image segmentation [30], [31], image classification [32], and other medical applications [33], [34]. This learning process is achieved through backpropagation, which is a feedback loop for computing the partial derivative of the cost function with respect to the network weights [35]. Initially, supervised deep learning methods were proposed [36], [37] to learn similarity features from the training data using different imaging modalities. Then, deep learning methods have been applied to solve the challenging multi-modal medical image registration problem where images from different image sensors are aligned together [38]–[42]. Further, unsupervised learning was developed as demand for faster registration procedures and to eliminate the challenges related to the ground truth data generation and optimization techniques [43]–[45]. Although our proposed method, iRegNet, uses an encoder-decoder-based method similar to [39] and [44], this is, to our best of knowledge, the first study to use the truth warped images as the target of the registration rather than the fixed image

which provides more precise information for the training process. Unsupervised approaches show promising registration results; however, it is still difficult to apply them to multi-modal registration of MRI and iUS applications since represented information originates from very distinct physical properties. Lately, CNN learning methods have been introduced as part of the Correction of Brain-shift with Intra-Operative Ultrasound challenge (CuRIOUS) [46] in conjunction with the Medical Image Computing and Computer-Assisted Intervention (MICCAI) [47], [48]. Overall, once the deep learning networks are trained, they can provide a faster registration than classical optimization methods, without the need for fine-tuning parameters at the test time, in addition to being more robust to outliers.

Our preliminary communication of this research work is presented in [49], where we investigated an initial deep learning-based method for automatic pre-operative MRI and interventional US registration based on the mean squared error (*MSE*) metric. A primary comparison was reported with three public classical non-learning methods namely, ANTs, NiftyReg, and deeds using only a single dataset. Here, we propose iRegNet, an automated deformable MRI to iUS registration workflow using deep learning, intending to provide considerably improved robustness and computational performance toward brain-shift compensation for assisting neurosurgeons intra-operatively. The contributions of this study include the following advancements:

- Presenting the two-step workflow of the proposed iRegNet method, which first takes two input volumes: pre-operative MRI (the moving image) and the iUS (the fixed image) as input. Then, the deep neural network generates the corresponding deformation field and corrects the brain-shifted MRI volume using deformable registration.

- Utilizing the truth warped images as the target of the registration rather than the fixed image in the conventional registration method, e.g., Voxelmorph [44]. This provides more accurate guided information for training iRegNet and, therefore, contributes to the overall accuracy of the registration results.

- Carrying out experiments using 36 patients from two publicly available multi-location databases: BITE and RESECT using three variations. The first variation includes training data from the BITE dataset, the second variation employs cases from the RESECT dataset, while a combination of both datasets cases is utilized in the third variation.

- Comprehensively evaluating the MRI to iUS registration results using two numerical metrics: the mean target registration errors (mTRE) and the computational processing time. Notably, almost two 3D MRI-iUS pairs per second can be registered on the same GPU using the proposed approaches.

- Competitive registration results when applying our methods on unseen MRI-iUS cases, which evidences the general applicability of our methods.

- A detailed comparison with the state-of-the-art non-learning- and learning-based registration algorithms across multi-site volumes.
- Qualitative analysis is performed (by two experienced neurosurgeons) highlighting the clinical applicability of our framework in neurosurgical guidance.

The remainder of the paper is structured as follows: The next section describes briefly medical image registration and our proposed MRI-iUS registration workflow. In Section III, experiments and the employed registration procedure are presented. Finally, experimental results on two datasets in multiple locations are discussed in Section IV, and conclusions are summarized in Section V.

II. METHODS

A. DEFORMABLE IMAGE REGISTRATION

Image registration is the process of finding spatial correspondences between two or more images [10], [50], [51]. Within the medical field, image registration is attractive for providing more information when the imaging data come from different sources and/or different modalities. The term deformable denotes that the images are related through non-linear spatial deformation and the resultant transformation not only includes rigid operations (such as rotation and translation) but also non-uniform operations like shearing. Consider two sets of images: the source or moving image I_M and the target or fixed image I_F. Then, the goal of deformable registration is finding the optimal deformation field ϕ that relates the two images while optimizing the energy function ε:

$$\varepsilon = S\left(I_F, I_M.\phi\right) + R\left(\phi\right) \tag{1}$$

where S quantifies the level of similarity between the I_M and I_F images, and the regularization term $R(\phi)$ allows a smooth transformation aiming to fulfill any user-specific requirements. In this study, we use the MRI as the moving image and iUS as the fixed image so that we could update the MRI to reflect the brain-shift intra-operatively.

B. LEARNING-BASED REGISTRATION FRAMEWORK

In this section, we describe the proposed registration workflow (presented in Fig. 1). Section B.1) presents the developed convolutional neural network (CNN). The loss functions of the CNN are illustrated in Section B.2), and the global optimization of the deformation field is explained in Section B.3).

1) DEEP NEURAL NETWORK ARCHITECTURE

Fig. 2 depicts the overall architecture of the proposed CNN utilized in our experiments. The proposed network is based on the U-Net structure [30], which has been widely utilized in various medical applications achieving competitive performance. 3D version of U-Net is introduced by Çiçek et al [52], in which 3D operations are applied instead of the standard 2D processes. Besides, several studies have demonstrated enhancements to the original U-Net [12], [31], [45].

Similar to the standard U-Net, our proposed network has an encoder-decoder architecture with an image analysis
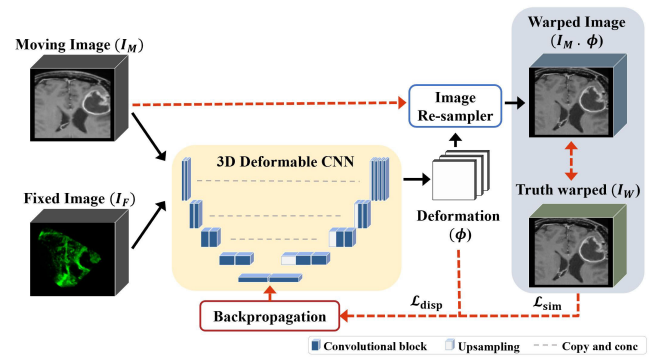

FIGURE 1. A representative workflow of the proposed MRI-iUS deformable registration approach, where dashed red arrows indicate the data flows only required in the training stage.
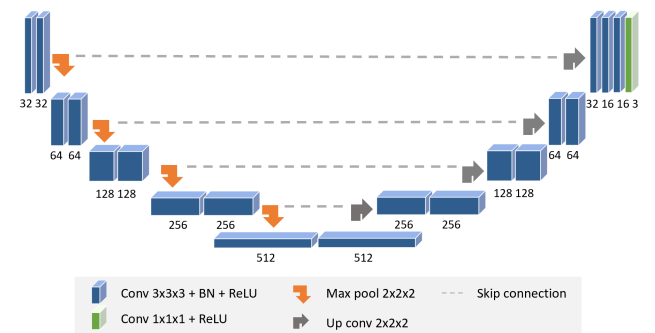

FIGURE 2. The enhanced 3D CNN architecture for predicting the deformation field ϕ. The network consists of 3D convolution with batch normalization layers (blue blocks), maximum pooling (orange arrows), up-sampling (grey arrows), and concatenate connections (dashed grey lines). The number of features is doubled in each step of the encoder part, while halved in the decoder part.

path (left side) and deformation estimation path (right side). As shown in Fig. 2, the feature analysis is designed as a 3D CNN with four repetitive down-sampling blocks. The input to the network is $128 \times 128 \times 128$ voxels with 2 channels of the MRI and iUS images. Each encoder block consists of two consecutive $3 \times 3 \times 3$ convolutional layers (unpadded convolutions) with a stride of 2, each followed by a rectified linear unit (ReLU) and batch normalization. At each down-sampling step, the number of feature maps is doubled, while the spatial dimension is halved using 3D spatial max pooling.

Initialization of all convolutional kernels is done by using the Glorot or Xavier uniform [53] with default bias set to zeros. It is worth noting that this contracting architecture is similar to the classical pyramid image registration scheme.

To restore the original image resolution, four up-sampling blocks are adopted in the deformation estimation path. Every step in the up-sampling path is composed of a $3 \times 3 \times 3$ transposed convolutional layer (up-convolution) with a stride of 2 followed by a ReLU and batch normalization. Dissimilar to the encoder, using up-convolution doubles the input spatial resolution and halves the number of feature maps. The high-level features in the encoding path are concatenated with the

corresponding low-level features in the decoding path via skip connections. As the output layer, a $1 \times 1 \times 1$ convolutional layer is incorporated to get the output deformation field with a dimension of $128 \times 128 \times 128$ in x, y, and z directions, respectively.

2) LOSS FUNCTIONS

The choice of the loss function plays a crucial role in our network training and contributes to the overall performance of the CNN. As illustrated in Fig. 1, the overall loss function $L_{overall}$ consists of two main elements (refer to Equation (2)). The similarity measurement between the resultant deformed image $(\phi.I_M)$ and the ground truth warped image I_W is denoted by L_{sim}, while L_{disp} represents the spatial deformation gradient error.

$$L_{overall} = L_{sim} + L_{disp} \tag{2}$$

In our experiments, we employ two distinct similarity metrics of *MSE* [54] and the local normalized correlation coefficient (*NCC*) [55] as L_{sim}. Let $I_M(p)$ and $I_W(p)$ represent a corresponding patch p in the moving and truth warped images, respectively. *MSE* and *NCC* are calculated as follows:

$$MSE(I_W, \phi.I_M)$$
$$= \frac{1}{|X|} \sum_{p \in X} ((I_W(p) - \phi.I_M(p)))^2 \tag{3}$$
$$NCC(I_W, \phi.I_M)$$
$$= \frac{1}{N} \sum_{p \in X}$$
$$\times \frac{\sum_i \left(I_W(p) - \overline{I_W(p)}\right) \sum_i \left(\phi.I_M(p) - \overline{\phi.I_M(p)}\right)}{\sqrt{\sum_i \left(I_W(p) - \overline{I_W(p)}\right)^2} \sqrt{\sum_i \left(\phi.I_M(p) - \overline{\phi.I_M(p)}\right)^2}} \tag{4}$$

where $I_W(p)$ denote the mean pixel intensities for the warped image. For MRI-iUS registration, it is very important to choose modality-invariant similarity metrics that can evaluate the similarity between MRI and iUS images after the deformable alignment. The *NCC* similarity is invariant to scaling and linear intensity variations, which makes it more preferable in our application. Similar to traditional registration approaches, the second loss works as a regularization term preventing a non-smooth deformation field. Let d denote the predicted spatial gradient and d_{truth} denote the ground truth gradient. Then, L_{disp} can be calculated as follows:

$$L_{disp} = \sum_{p \in X} \|d_{truth}(p) - d(p)\| \tag{5}$$

3) GLOBAL OPTIMIZATION

Traditionally, the optimization of the deformation field has been formulated as an iterative pair-wise optimization problem (refer to equation (1)). This is a computationally expensive problem that consumes large processing time and may last for hours for a single pair depending on the used CPU. In contrast, deep learning methods recast the classical optimization problem into a problem of cost function estimation [35]. In other words, this formulates the problem to find

TABLE 1. A detailed description of the two databases used in this study.

		BITE	RESECT
(a) Imaging Site		Montreal Neurological Institute, Montreal, Canada	St. Olavs University Hospital, Trondheim, Norway
(b) Study Characteristics	N. of Patients	14	22
	Tumor Type	LGG (4) HGG (9)	LGG (22)
	N. of Landmarks	355	338
(c) MRI Protocol	MRI Scanner	1.5T General Electric Signa EXCITE	3T Siemens Magnetom Skyra and 1.5T Siemens Magnetom Avanto
	Date of Acquisition	Avg. 17 days before surgery (1–72 days)	1 day before surgery
	MRI Modalities	T1w Gd-enhanced	T1w Gd-enhanced and T2w fluid-attenuated inversion recovery (FLAIR)
	MRI Resolution	$256 \times 256 \times 256$	$256 \times 256 \times 192$
	Voxel Size	$1 \times 1 \times 1$ mm^3	$1 \times 1 \times 1$ mm^3
(d) iUS Protocol	iUS Probe	Phased-array transducer	12FLA-L linear probe
	iUS Frequencies	7-4 MHz	6-12 MHz
	iUS Resolution	$0.3 \times 0.3 \times 0.3$ mm^3	$0.14 \times 0.14 \times 0.14$ mm^3 to $0.24 \times 0.24 \times 0.24$ mm^3

a function that takes a pair of MRI-iUS images and directly computes the output deformation field using backpropagation, which makes our method optimize over the whole training set moving away from expensive iterative optimization.

III. EXPERIMENTS

A. DATA

In this study, we tested the proposed method on two public multi-center databases, which are BITE [56] and RESECT [57]. BITE is the first online dataset for tracked 3D iUS volumes of the brain alongside pre-operative MRI images. It contains 14 patients with either low-grade glioma (LGG) or high-grade glioma (HGG) from the Montreal Neurological Institute, Canada. Nevertheless, the technology used to collect the iUS in the BITE dataset is no longer up-to-date and recent US scanners provide improved quality and higher resolution images. Consequently, the RESECT was proposed to overcome this problem and help, therefore, develop image registration techniques for brain-shift compensation. The dataset contains pre-operative MRI and iUS images from 22 patients with LGG who have received surgeries at St. Olavs University Hospital, Norway. Table 1 gives detailed information on the applied datasets with a wide variety of (a) data acquiring locations, (b) patient and tumor details, and (c) applied MRI and US protocols.

Expert-labeled anatomical markers were provided for both databases, to facilitate the baseline evaluation of MRI to
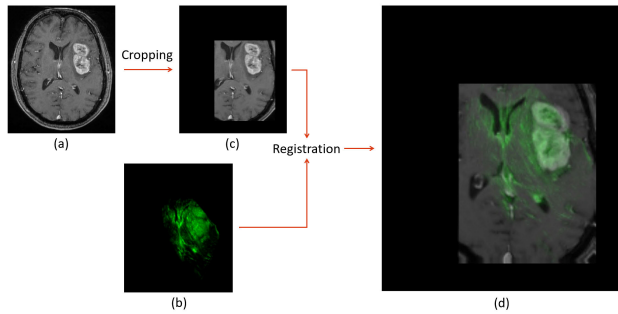
FIGURE 3. Our MRI-iUS registration procedure (a) Input MRI; (b) Input iUS; (c) Cropped MRI; (d) An overlap between iUS and corrected MRI.

iUS registration. The procedure of generating these landmarks highly depends on the employed datasets. For the BITE dataset, homologous landmark points were chosen manually by at least two experts. An average of nine landmarks was provided in the BITE database for each patient. For the RESECT dataset, more landmarks were provided which may lead to better validation of registration accuracy. In both datasets, the package named 'register', included in the MINC toolkit [58], was used to visualize the 3D MRI-US pairs and produce the homologous landmarks. It should be noted that this process was performed only in the training stage, however, during the inference, no landmarks are utilized to get the corrected MRI volumes. For each pair in BITE, we used the homologous landmarks from the first two experts (D.L.C. and L.M.) without the third expert's labels since they tagged only up to patient #6 [59].

B. REGISTRATION PROCEDURE
As listed in Table 1, it is evident that there are several dissimilarities between the two datasets in terms of imaging locations, study characteristics, followed MRI and iUS protocols, and, therefore, a preprocessing step is essential before performing the MRI-iUS registration. First, the ultrasound images are resampled to the isotropic $1 \times 1 \times 1$ mm^3 voxel size, same as the MRI spatial resolution.

Second, we pad iUS images to $128 \times 128 \times 128$ voxels to make them suitable for the deep neural network input. Third, we use the initial alignment of MRI images to iUS data and then crop the MRI to match the field of view of the iUS, as shown in Fig. 3. Fourth, z-score normalization is applied by subtracting the mean value and dividing by the standard deviation individually for each input volume. Fifth, an affine MRI to iUS alignment is achieved using the MINC toolkit [58] to focus on the non-linear misalignment. Finally, truth deformation fields for all patients were computed using the software named 'register', included in the MINC toolkit so that the deformation field gradient error L_{disp} could be estimated (refer to Section II B.2).

C. EXPERIMENTAL SETUP AND EVALUATION
Our CNN models are built using Keras library with TensorFlow backend [12]. The experiments were conducted on

an AMD Ryzen 2920X (32M Cache, 3.50 GHz) CPU with 32 GB RAM and a single NVIDIA RTX 2080Ti GPU 11GB GDDR6. For training our networks, the ADAM optimization technique is adopted with an initial learning rate set to 0.0001, and batch size set to 2. All models were trained for 500 epochs, with one epoch being defined as an iteration over 500 mini-batches.

The proposed approach was evaluated using three configurations: The first configuration, referred to as *Model BITE* or *Model B*, involved training on the BITE dataset only. The second configuration, referred to as *Model RESECT* or *Model R*, involved training on the RESECT dataset only. The last configuration, referred to as *Model Combined* or *Model C*, involved training on both BITE and RESECT datasets. It is important to note that a total of six experiments, which use affinely aligned MRI-iUS images, were conducted for the registration of MRI-iUS based on alternating NCC and MSE as a similarity measurement for training the CNN. For the training phase, 11, 17, and 28 pairs of MRI and iUS images are used for the *Model B*, *Model R*, and *Model C*, respectively. Whereas 3, 5, and 8 pairs of MRI and iUS images are used for validation in the same order.

The two datasets, BITE and RESECT, provide expert-annotated landmarks for each corresponding MRI-iUS pair (as summarized in Table 1). In line with previous studies [13], [14], [16]–[24], [47], [48], [60], we use the mTRE, which represents the average pair-wise distance between the corresponding points in MRI and iUS volumes after registration. Let m and u denote the expert-labeled corresponding annotations in the MRI and iUS volumes, respectively. The *mTRE* of n corresponding landmarks, following the registration, is calculated as follows:

$$mTRE = \frac{1}{n}\sum_{i=1}^{n} \|\phi(m_i) - u_i\| \qquad (6)$$

where $\|r\|$ is the L^2 norm of the vector r.

IV. RESULTS AND DISCUSSION
A. QUANTITATIVE REGISTRATION RESULTS
Tables 2 and 3 summarize the mTREs of pre-and post-registration of the three proposed methods for all the trained 14 BITE and 22 RESECT cases, individually. The last row of each table denotes a summary of the results over the listed cases. The results show that the proposed methods provide a major improvement over the initial alignment. For the BITE database, our algorithms reduced the initial mTRE from $(4.18 \pm 1.84$ mm$)$ to a range from $(1.47 \pm 0.61$ mm$)$ to $(2.00 \pm 0.45$ mm$)$ based on the applied configuration. Similarly, average mTRE from $(0.84 \pm 0.16$ mm$)$ to $(2.50 \pm 0.66$ mm$)$ was achieved on the RESECT database starting with an initial mTRE value of $(5.35 \pm 4.19$ mm$)$. Notably, the use of NCC as a similarity metric had a great impact on the registration accuracy as all NCC-based models show an improvement over the standard MSE-based methods. This proves the effectiveness of using NCC for multi-modal registration as it is intensity and scaling invariant.

TABLE 2. Pre-and post-registration TREs for our proposed models in the BITE dataset. *Model B, Model R, and Model C* represent our proposed models trained on the BITE, RESECT, and both datasets, correspondingly. Test cases are shown in *bold underlined* and the lowest error in each row is highlighted in *bold*.

Case	INITIAL	Model B MSE	Model B NCC	Model R MSE	Model R NCC	Model C MSE	Model C NCC
Case01	5.88(2.31)	1.42(0.79)	1.17(0.55)	1.82(0.96)	1.83(0.98)	1.82(0.97)	**1.04(0.58)**
Case02	6.06(1.61)	1.14(0.67)	1.27(0.77)	1.46(0.83)	1.54(0.82)	1.39(0.80)	**0.97(0.45)**
Case03	8.91(2.02)	1.57(1.12)	1.39(0.87)	2.24(1.23)	2.19(1.28)	2.11(1.26)	**1.22(0.87)**
Case04	3.87(1.19)	0.91(0.41)	1.01(0.51)	1.57(0.86)	1.50(0.72)	1.45(0.69)	**0.90(0.47)**
Case05	2.57(1.61)	1.43(1.09)	1.50(1.00)	2.02(1.51)	2.04(1.50)	2.00(1.51)	**1.21(0.80)**
Case06	2.24(1.05)	1.21(0.57)	1.24(0.57)	1.57(0.68)	1.52(0.63)	1.50(0.65)	**1.08(0.50)**
Case07	3.02(1.58)	2.15(0.95)	2.16(0.77)	2.15(0.79)	**1.99(0.81)**	1.99(0.76)	2.08(0.80)
Case08	3.75(1.97)	**1.36(0.67)**	1.61(0.81)	2.31(1.11)	2.22(1.06)	2.17(1.03)	1.37(0.69)
Case09	5.08(1.33)	1.60(0.71)	1.87(1.16)	2.43(1.14)	2.48(1.12)	2.39(1.07)	**1.49(0.81)**
Case10	2.99(1.34)	1.80(0.82)	1.59(0.79)	**1.41(0.69)**	1.45(0.73)	1.44(0.73)	1.75(0.88)
Case11	1.51(0.73)	1.60(0.84)	1.47(0.73)	1.34(0.64)	**1.32(0.68)**	**1.32(0.68)**	1.48(0.69)
Case12	3.68(1.85)	3.14(2.60)	2.91(2.45)	2.74(1.75)	2.70(1.77)	**2.66(1.74)**	3.38(3.28)
Case13	5.13(2.73)	1.81(1.35)	1.67(1.08)	2.51(1.30)	2.59(1.23)	2.40(1.30)	**1.40(0.87)**
Case14	3.78(1.23)	1.34(0.64)	1.42(0.78)	2.44(0.91)	2.31(0.85)	2.24(0.87)	**1.18(0.43)**
mTRE	4.18(1.84)	1.61(0.52)	1.59(0.46)	2.00(0.45)	1.98(0.44)	1.92(0.42)	**1.47(0.61)**

TABLE 3. Pre- and post-registration TREs for our proposed models in the RESECT dataset. *Model B, Model R, and Model C* represent our proposed models trained on the BITE, RESECT, and both datasets, correspondingly. Test cases are shown in *bold underlined* and the lowest error in each row is highlighted in *bold*.

Case	INITIAL	Model B MSE	Model B NCC	Model R MSE	Model R NCC	Model C MSE	Model C NCC
Case01	1.81(0.84)	3.71(1.30)	2.07(0.87)	1.17(0.74)	**1.13(0.58)**	**1.13(0.58)**	1.42(0.76)
Case02	5.70(1.39)	2.79(0.83)	2.67(0.85)	1.05(0.43)	**0.72(0.37)**	1.15(0.57)	0.86(0.37)
Case03	9.56(0.52)	3.30(0.97)	1.96(0.68)	0.91(0.38)	**0.86(0.34)**	0.94(0.37)	0.94(0.37)
Case04	2.45(0.67)	**0.89(0.39)**	1.04(0.40)	1.26(0.46)	1.04(0.40)	1.04(0.40)	1.72(0.61)
Case05	12.03(1.05)	2.73(0.97)	1.77(0.61)	0.79(0.32)	**0.73(0.37)**	1.00(0.47)	0.82(0.38)
Case06	3.25(0.63)	2.75(0.93)	1.70(0.57)	**0.85(0.32)**	0.85(0.29)	0.91(0.32)	0.89(0.30)
Case07	1.86(1.06)	2.47(0.90)	2.18(0.66)	0.97(0.41)	**0.73(0.32)**	1.24(0.56)	0.81(0.37)
Case08	2.65(0.86)	3.14(0.91)	2.10(0.78)	1.29(0.49)	1.28(0.43)	**1.21(0.45)**	1.60(0.60)
Case12	19.71(0.72)	3.02(1.14)	1.85(0.78)	0.91(0.30)	**0.82(0.29)**	0.96(0.30)	0.83(0.35)
Case13	4.56(1.29)	2.13(0.65)	1.64(0.48)	0.93(0.39)	**0.85(0.30)**	1.01(0.40)	0.89(0.34)
Case14	3.02(0.61)	2.63(0.88)	2.55(0.87)	1.11(0.42)	**1.05(0.39)**	**1.05(0.39)**	1.17(0.36)
Case15	3.23(1.28)	2.70(0.76)	2.09(0.61)	0.95(0.51)	**0.85(0.45)**	1.30(0.55)	1.00(0.46)
Case16	3.39(0.83)	2.32(0.72)	1.66(0.42)	**0.68(0.20)**	0.71(0.24)	0.90(0.34)	0.74(0.24)
Case17	6.37(0.75)	2.48(1.07)	1.63(0.80)	0.73(0.27)	**0.69(0.29)**	1.02(0.42)	0.73(0.25)
Case18	3.57(0.93)	2.27(0.90)	1.32(0.40)	**0.68(0.25)**	0.69(0.28)	0.81(0.31)	0.72(0.30)
Case19	3.29(1.25)	1.93(1.09)	1.65(0.45)	0.78(0.39)	**0.64(0.26)**	0.80(0.38)	0.68(0.29)
Case21	4.56(0.71)	2.92(0.90)	1.84(0.62)	0.82(0.28)	**0.78(0.20)**	1.05(0.47)	0.82(0.27)
Case23	7.02(1.02)	1.75(0.95)	1.68(0.58)	**0.65(0.21)**	0.70(0.26)	0.71(0.26)	0.70(0.24)
Case24	1.09(0.40)	1.87(0.95)	1.68(0.46)	0.68(0.26)	**0.60(0.28)**	0.71(0.26)	0.64(0.29)
Case25	10.06(2.27)	1.52(0.72)	1.41(0.53)	1.11(0.43)	**0.94(0.45)**	**0.94(0.45)**	1.60(0.54)
Case26	2.82(0.81)	3.58(1.31)	2.68(0.90)	0.77(0.29)	0.84(0.27)	0.97(0.42)	**0.83(0.31)**
Case27	5.77(0.66)	2.05(0.91)	1.63(0.74)	1.00(0.38)	**0.89(0.33)**	1.15(0.42)	1.00(0.35)
mTRE	5.35(4.19)	2.50(0.66)	1.85(0.40)	0.91(0.19)	**0.84(0.16)**	1.00(0.16)	0.97(0.32)

From the BITE results, it is important to note that the most accurate results were generated by *Model C NCC*. This result emphasizes that utilizing more training data in deep learning often leads to a performance enhancement. However, this did not have the same effect on the RESECT dataset wherein *Model C NCC* ranked third after *Model R* versions. This might be due to the difference in the two databases, refer to Table 1, resulting in a model struggling to extract common features. Still, *Model C NCC* improved significantly the initial mTRE from (5.35 ± 4.19 mm) to (0.84 ± 0.16 mm). Obviously, the results indicated that that deep learning approach can perform automatic accurate

deformable MRI to iUS image registration, and thus could be used in image-guided neurosurgical interventions.

B. GENERALITY EVALUATION

One of our main goals is to build an automated learning model that can be applied to multi-site data without database-specific model parameters fine-tuning. To achieve this goal, we evaluated the three proposed models: *Model B, Model R, and Model C* on both utilized databases. For instance, *Model B* was trained using the BITE dataset only, therefore, testing this model on the other dataset of RESECT would give
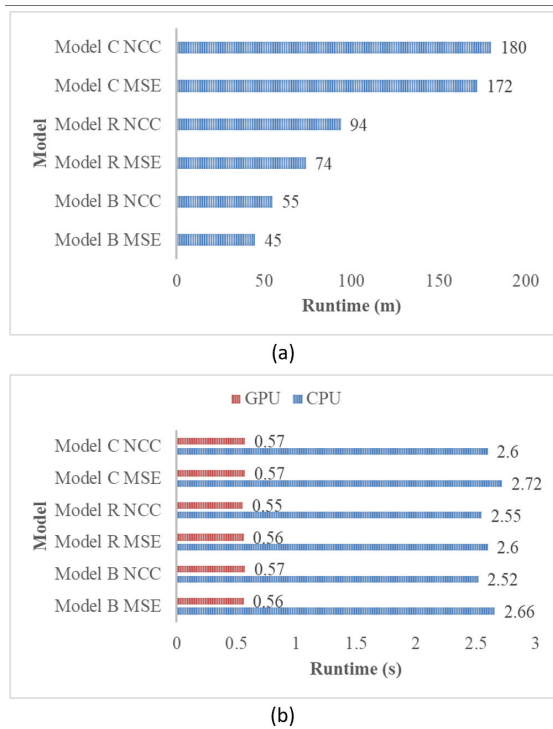
(a)

(b)

FIGURE 4. Processing time analysis for the proposed approaches on two different multiple sites datasets. (a) Training time in minutes; (b) Test time in seconds using CPU (in Blue) and GPU (in Red).

FIGURE 5. A comparison of the registration error (mTRE) for our proposed iRegNet methods and the state-of-the-art methods on the BITE dataset.

FIGURE 6. A comparison of the registration error (mTRE) for our proposed iRegNet methods and the state-of-the-art methods on the RESECT dataset.

us a general idea about how our method may generalize with other unseen datasets.

Remarkably, *Model B* and *Model B NCC* decreased the initial mTRE from (5.35 ± 4.19 mm) to only (2.50 ± 0.66 mm) and (1.85 ± 0.40 mm) experienced on untrained RESECT dataset. Likewise, the two variations of *Model R*, trained on the RESECT dataset only, delivered astonishing results on the BITE dataset with average mTRE from (2.00 ± 0.45 mm) to (1.98 ± 0.44 mm) over the initial (4.18 ± 1.84 mm). These findings further strengthened our conviction that deep learning-based models can deliver competitive MRI to iUS registration results even if they are not trained on the evaluated data, which shows therefore a promise for use during brain surgery.

C. PROCESSING TIME ANALYSIS
Fig. 4 shows the computation time for the training stage (Fig. 4 (a)) and the test stage (Fig. 4 (b)). The most remarkable result is that the first configuration, *Model B* and *Model B NCC*, has the lowest training time of 45 and 55 minutes, respectively, because they are trained on the BITE dataset containing only 14 patients. On the other hand, the largest training times of 172 and 180 minutes are obtained by the third setup, *Model C* and *Model C NCC*, which use a total of 36 patients from both datasets. It becomes notable that incorporating the NCC as the similarity measurement leads to an increase of the training time with 5 to 26% over the MSE versions, but the test time remains approximately constant.
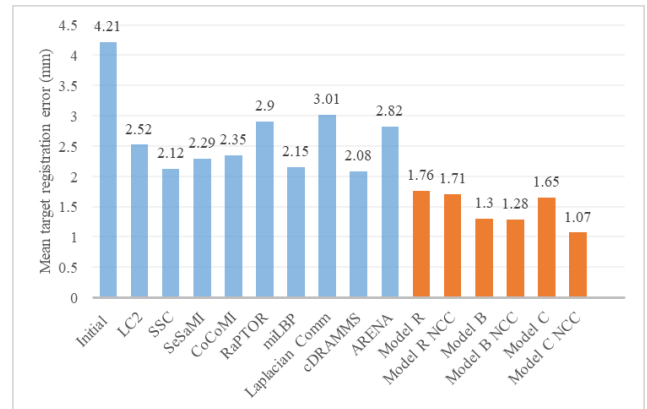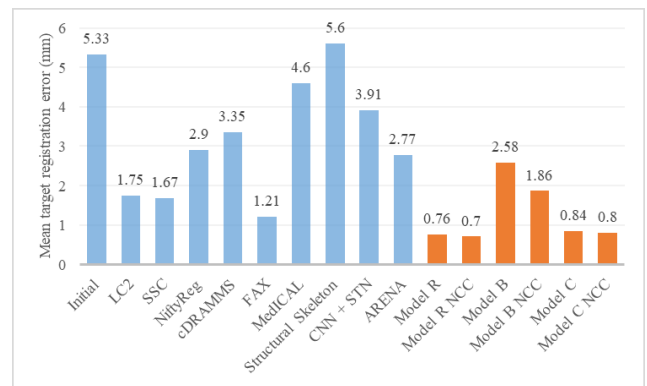
Overall, the three approaches provide similar processing test times of approximately 0.5 seconds on the GPU and 2.6 seconds on the CPU which provides additional support for using iRegNet in time-critical image-guided interventions.

D. COMPARISON WITH OTHER MRI-IUS STUDIES
Fig. 5 shows the initial and final landmarks errors for the proposed iRegNet methods and methodologies found in the literature for MRI-iUS registration, performed on the BITE database. To assess our proposed methods, we compare them against other MRI-iUS registration algorithms proposed for the brain-shift compensation: LC^2 [24], SSC [25], SeSaMI [14], CoCoMI [14], RaPTOR [16], miLBP [17], Laplacian Comm [26], cDRAMMS [27], and Arena [18]. The results obtained indicate that our methods, highlighted in *orange*, outperform other evaluated competing techniques. In particular, the configuration *Model C NCC* ranked first for the BITE with an mTRE (1.47 ± 0.61 mm) with a 0.61 mm margin smaller than the best performing method cDRAMMS [27].

Additional comparison of our registration methods against other approaches using pre-operative MRI and pre-resection US images from the RESECT database are presented
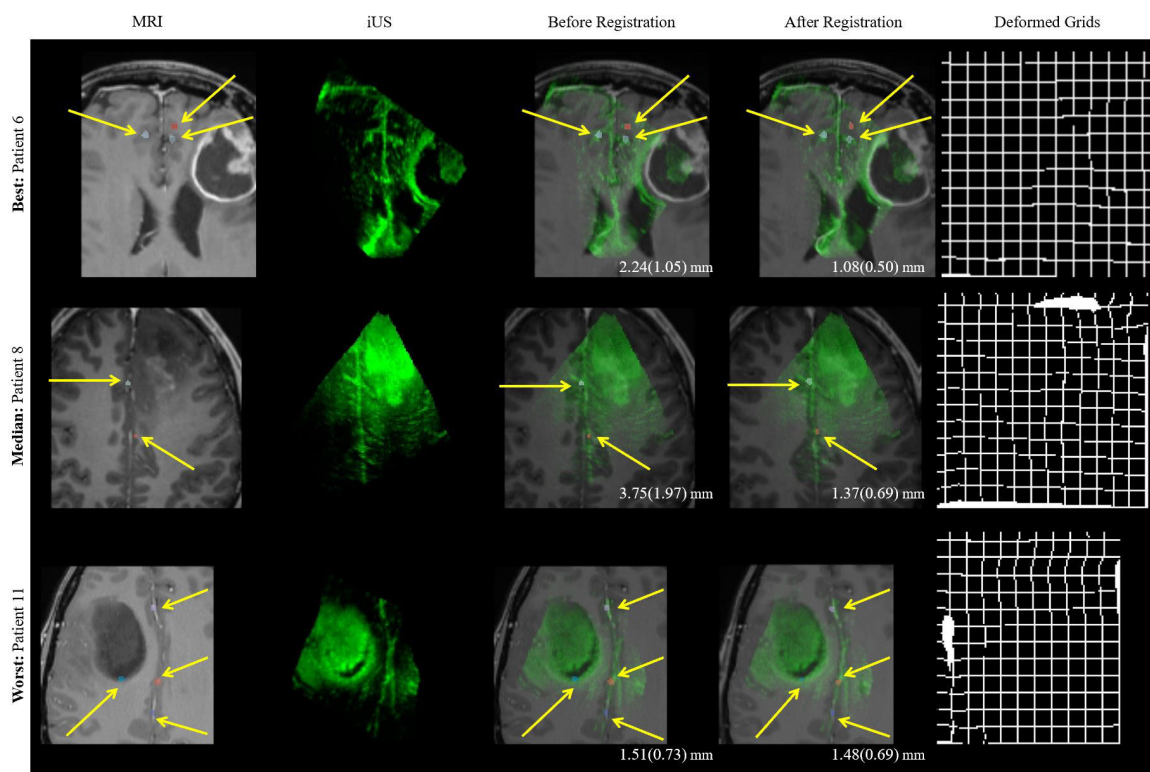
FIGURE 7. Alignment of pre-operative MRI (gray color mode) to iUS (green color mode) in three different cases from BITE (cases #6, #8, and #11). Row designations: pre-operative T2-FLAIR MRI, intra-operative US, initial misaligned MRI over iUS before registration, the final aligned MRI over iUS after registration, and the deformed grids. Yellow arrows indicate expert-labeled landmarks while mTRE values are shown (bottom right).

in Fig. 6. iRegNet methods are compared to conventional studies: LC^2 [19], SSC [20], NiftyReg [22], cDRAMMS [21], MedICAL [23], Structural Skeleton [60], ARENA [18] as well as learning studies: FAX [47], CNN + STN [48]. It is important to note that the LC^2 algorithms applied to BITE utilized different configurations than the one applied to RESECT. In [24], the algorithm aligns 2D US to 3D MRI volumes initialized with a rigid registration and a smaller patch sizes of 2 to 24, while in [19], a non-linear optimization algorithm was initialized with a translation before the rigid registration and the patch size is larger with 7^3 voxels. Similarly, the SSC methods in [25] and [20] are separate from each other. In [20], the authors set the parameters for the discrete optimization with a complex 10^7 degrees of freedom. On the other hand, the graph is simplified in [25] and contains no loops leading to a faster and smoother transformation.

As can be seen from Fig. 6, *Model R* variants rank first on the RESECT dataset with average mTRE (0.84 ± 0.16 to 0.91 ± 0.19 mm) followed by the learning-based method FAX with mTRE of (1.21 ± 0.55 mm). Although team FAX reported comparable results, this method failed to obtain similar results on the test dataset of the CuRIOUS challenge [46], which presumably is due to an overfit over the training images. In contrast, *Model B* and *Model B NCC* enhanced the initial mTRE of RESECT by 2.85 and 3.50 mm in turn,

TABLE 4. Statistical assessment of the MRI-iUS alignment of 36 cases by two expert neurosurgeons.

	ASSESSMENT			
Neurosurgeon	**Limited**	**Fair**	**Good**	**Excellent**
#1	4	3	13	16
#2	4	6	14	12
Total	8	9	27	28

however, they failed to provide competitive outcomes. This implies that the accuracy of deep learning approaches does seem to depend on the size of the available training data.

E. QUALITATIVE ANALYSIS BY NEUROSURGEONS

Two experienced neurosurgeons (Z. A.) and (M. S.) with eight and five years of clinical practice, respectively, visually inspected the MRI-iUS registration results individually and rated the results based on the tumor boundaries and other brain structures, such as sulci and falx. Table 4 summarizes their qualitative analysis. It is worth mentioning that only 11% of alignments were classified as "limited" (no improvements over the initial registration), and 8% or 17%, respectively, of aligned results were "fair" (minor improvements),
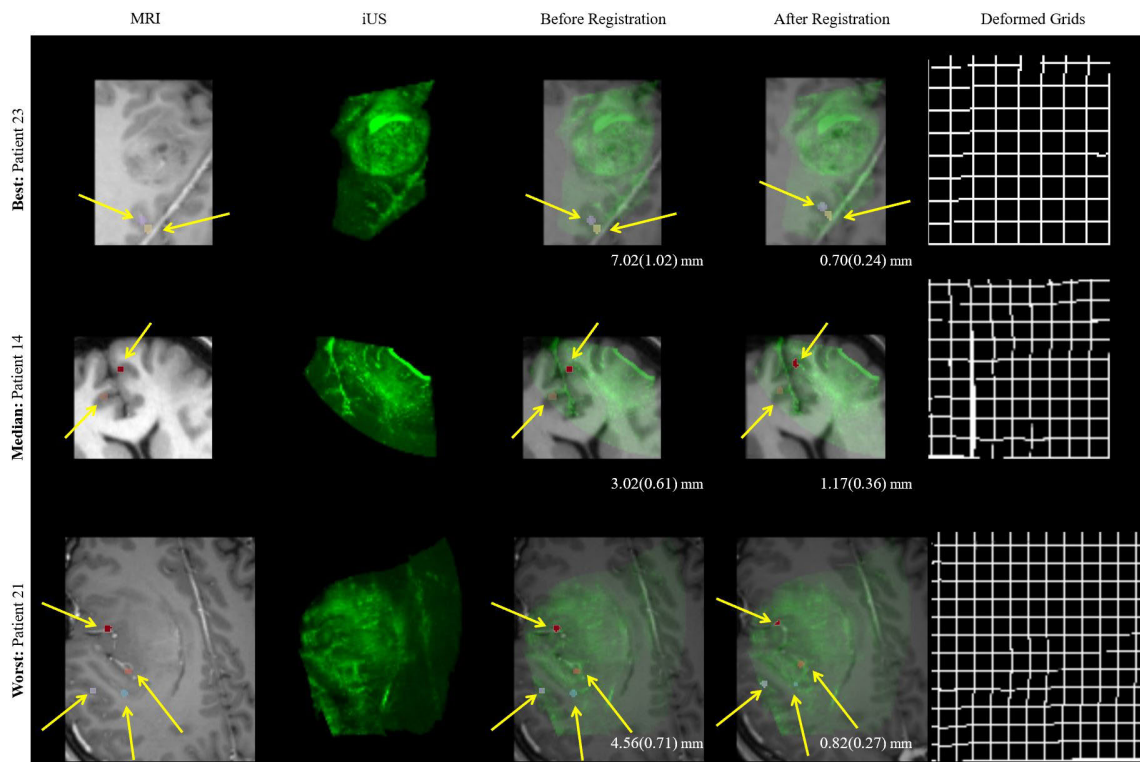
FIGURE 8. Alignment of pre-operative MRI (gray color mode) to iUS (green color mode) in three different cases from RESECT (cases #23, #14, and #21). Row designations: pre-operative T2-FLAIR MRI, intra-operative US, initial misaligned MRI over iUS before registration, and the final aligned MRI over iUS after registration, and the deformed grids. Yellow arrows indicate expert-labeled landmarks while mTRE values are shown (bottom right).

36% or 39%, respectively, of alignments were "good" (major improvements), and 44% or 33%, respectively, of alignments were "excellent" (little or no visible misalignment).

Fig. 7 and Fig. 8 display the results of aligning MRI to iUS using our best method, namely *Model C NCC,* for six different patients: BITE (cases #6, #8, and #11) and RESECT (cases #23, #14, and #21), correspondingly. The cases are selected as best, median, and worst according to their qualitative evaluation as given in Table 4. In each figure, rows provide pre-operative MRI, interventional US, initial alignment of both images before registration, and overlap of corrected MRI over iUS after applying iRegNet, correspondingly. Similar to other studies, the raters confirm that the quality of the used US images in the BITE dataset is rather limited as shown in case #8 in Fig. 7.

The results of this study demonstrated that iRegNet, *Model C NCC*, yields better registration results (last row) than the initial misaligned MRI and iUS pairs (third row). Although widely accepted, it suffers from a comparable larger training time of 180 minutes, however, this is only apparent in the training stage while obtaining a very competitive inference time of about half-second on GPU-based implementation. Another limitation of this implementation is that this improvement may be unclear in few cases, such as Case12 from the BITE dataset. A popular explanation is

that the initial alignment has a small brain-shift that makes it difficult to observe. Overall, this analysis yields an overview of the potential clinical applicability of our method regarding the accuracy and quality of the registration outputs.

V. CONCLUSION

We presented iRegNet as an automated fast and robust deformable method for pre-operative MRI to pre-resection iUS registration for compensating brain-shift phenomenon. In six experiments, our proposed method has been successfully tested and evaluated on 36 cases from two multi-location datasets, validating the registration performance qualitatively and quantitatively. Notably, iRegNet achieved considerable performance and computational efficiency even with untrained cases, demonstrating the generality of our proposed method. Compared with other registration methods, iRegNet achieved the best accuracy results in terms of the mean TRE with values of $(1.47 \pm 0.61$ and 0.84 ± 0.16 mm) for the utilized BITE and RESECT datasets, respectively, as illustrated in Table 2 and Table 3. Furthermore, the qualitative results indicate that the registered MRI-iUS pairs have a significant improvement over their initial alignment. Also, our proposed iRegNet achieved significant performance on multi-center data and is therefore a potentially promising automatic registration algorithm for use with IGN systems.

Moreover, iRegNet is flexible, modality-, anatomy-invariant, and therefore could be used in a wide range of medical image analysis and processing surgical procedures.

Further research should be done to investigate the optimal cropping radius for MRI images so that the missing data are as few as possible. Automating this procedure would further contribute towards rendering iRegNet an end-to-end pipeline.

COMPLIANCE WITH ETHICAL STANDARDS

Conflict of Interest: The authors have no conflict of interest to declare.

Ethical Consent: The authors did not perform any experiments or clinical trials on animals or patients.

Code Availability: The code of this study is available upon request of the corresponding author Ramy A. Zeineldin (ramy.zeineldin@ieee.org).

REFERENCES

[1] R. C. Miner, "Image-guided neurosurgery," *J. Med. Imag. Radiat. Sci.*, vol. 48, no. 4, pp. 328–335, Dec. 2017, doi: 10.1016/j.jmir.2017.06.005.

[2] J. Coburger and C. R. Wirtz, "Fluorescence guided surgery by 5-ALA and intraoperative MRI in high grade glioma: A systematic review," *J. Neuro-Oncol.*, vol. 141, no. 3, pp. 533–546, Feb. 2019, doi: 10.1007/s11060-018-03052-4.

[3] C. Schulz, S. Waldeck, and U. M. Mauer, "Intraoperative image guidance in neurosurgery: Development, current indications, and future trends," *Radiol. Res. Pract.*, vol. 2012, May 2012, Art. no. 197364, doi: 10.1155/2012/197364.

[4] M. Bucki, C. Lobos, and Y. Payan, "Framework for a low-cost intra-operative image-guided neuronavigator including brain shift compensation," in *Proc. 29th Annu. Int. Conf. IEEE Eng. Med. Biol. Soc. (EMBS)*, Aug. 2007, pp. 872–875.

[5] E. De Momi, G. Ferrigno, G. Bosoni, P. Bassanini, P. Blasi, G. Casaceli, D. Fuschillo, L. Castana, M. Cossu, G. Lo Russo, and F. Cardinale, "A method for the assessment of time-varying brain shift during navigated epilepsy surgery," *Int. J. Comput. Assist. Radiol. Surg.*, vol. 11, no. 3, pp. 473–481, Mar. 2016, doi: 10.1007/s11548-015-1259-1.

[6] J. Coburger, R. W. König, A. Scheuerle, J. Engelke, M. Hlavac, D. R. Thal, and C. R. Wirtz, "Navigated high frequency ultrasound: Description of technique and clinical comparison with conventional intracranial ultrasound," *World Neurosurg.*, vol. 82, nos. 3–4, pp. 366–375, Sep. 2014, doi: 10.1016/j.wneu.2014.05.025.

[7] C. DeLorenzo, X. Papademetris, L. H. Staib, K. P. Vives, D. D. Spencer, and J. S. Duncan, "Image-guided intraoperative cortical deformation recovery using game theory: Application to neocortical epilepsy surgery," *IEEE Trans. Med. Imag.*, vol. 29, no. 2, pp. 322–338, Feb. 2010, doi: 10.1109/TMI.2009.2027993.

[8] I. J. Gerard, M. Kersten-Oertel, J. A. Hall, D. Sirhan, and D. L. Collins, "Brain shift in neuronavigation of brain tumors: An updated review of intra-operative ultrasound applications," *Frontiers Oncol.*, vol. 10, p. 3390, Feb. 2021, doi: 10.3389/fonc.2020.618837.

[9] D. Miller, L. Benes, and U. Sure, "Stand-alone 3D-ultrasound navigation after failure of conventional image guidance for deep-seated lesions," *Neurosurgical Rev.*, vol. 34, no. 3, pp. 381–388, Jul. 2011, doi: 10.1007/s10143-011-0314-9.

[10] A. Sotiras, C. Davatzikos, and N. Paragios, "Deformable medical image registration: A survey," *IEEE Trans. Med. Imag.*, vol. 32, no. 7, pp. 1153–1190, Jul. 2013, doi: 10.1109/TMI.2013.2265603.

[11] J. Liu, G. Singh, S. Al'Aref, B. Lee, O. Oleru, J. K. Min, S. Dunham, M. R. Sabuncu, and B. Mosadegh, "Image registration in medical robotics and intelligent systems: Fundamentals and applications," *Adv. Intell. Syst.*, vol. 1, no. 6, Oct. 2019, Art. no. 1900048, doi: 10.1002/aisy.201900048.

[12] G. Haskins, U. Kruger, and P. Yan, "Deep learning in medical image registration: A survey," *Mach. Vis. Appl.*, vol. 31, nos. 1–2, pp. 1–18, Feb. 2020, doi: 10.1007/s00138-020-01060-x.

[13] D. De Nigris, D. L. Collins, and T. Arbel, "Fast rigid registration of pre-operative magnetic resonance images to intra-operative ultrasound for neurosurgery based on high confidence gradient orientations," *Int. J. Comput. Assist. Radiol. Surg.*, vol. 8, no. 4, pp. 649–661, Jul. 2013, doi: 10.1007/s11548-013-0826-6.

[14] H. Rivaz, Z. Karimaghaloo, and D. L. Collins, "Self-similarity weighted mutual information: A new nonrigid image registration metric," *Med. Image Anal.*, vol. 18, no. 2, pp. 343–358, Feb. 2014, doi: 10.1016/j.media.2013.12.003.

[15] H. Rivaz, Z. Karimaghaloo, V. S. Fonov, and D. L. Collins, "Nonrigid registration of ultrasound and MRI using contextual conditioned mutual information," *IEEE Trans. Med. Imag.*, vol. 33, no. 3, pp. 708–725, Mar. 2014, doi: 10.1109/TMI.2013.2294630.

[16] H. Rivaz, S. J.-S. Chen, and D. L. Collins, "Automatic deformable MR-ultrasound registration for image-guided neurosurgery," *IEEE Trans. Med. Imag.*, vol. 34, no. 2, pp. 366–380, Feb. 2015, doi: 10.1109/TMI.2014.2354352.

[17] D. Jiang, Y. Shi, D. Yao, M. Wang, and Z. Song, "MiLBP: A robust and fast modality-independent 3D LBP for multimodal deformable registration," *Int. J. Comput. Assist. Radiol. Surg.*, vol. 11, no. 6, pp. 997–1005, Jun. 2016, doi: 10.1007/s11548-016-1407-2.

[18] N. Masoumi, Y. Xiao, and H. Rivaz, "ARENA: Inter-modality affine registration using evolutionary strategy," *Int. J. Comput. Assist. Radiol. Surg.*, vol. 14, no. 3, pp. 441–450, Mar. 2019, doi: 10.1007/s11548-018-1897-1.

[19] W. Wein, "Brain-shift correction with image-based registration and landmark accuracy evaluation," in *Simulation, Image Processing, and Ultrasound Systems for Assisted Diagnosis and Navigation* (Lecture Notes in Computer Science). Springer, 2018, ch. 17, pp. 146–151.

[20] M. P. Heinrich, "Intra-operative ultrasound to MRI fusion with a public multimodal discrete registration tool," in *Simulation, Image Processing, and Ultrasound Systems for Assisted Diagnosis and Navigation* (Lecture Notes in Computer Science). Springer, 2018, ch. 19, pp. 159–164.

[21] I. Machado, M. Toews, J. Luo, P. Unadkat, W. Essayed, E. George, P. Teodoro, H. Carvalho, J. Martins, P. Golland, S. Pieper, S. Frisken, A. Golby, W. Wells, III, and Y. Ou, "Deformable MRI-ultrasound registration via attribute matching and mutual-saliency weighting for image-guided neurosurgery," in *Simulation, Image Processing, and Ultrasound Systems for Assisted Diagnosis and Navigation* (Lecture Notes in Computer Science). Springer, 2018, ch. 20, pp. 165–171.

[22] D. Drobny, T. Vercauteren, S. Ourselin, and M. Modat, "Registration of MRI and iUS data to compensate brain shift using a symmetric block-matching based approach," in *Simulation, Image Processing, and Ultrasound Systems for Assisted Diagnosis and Navigation* (Lecture Notes in Computer Science). Springer, 2018, ch. 21, pp. 172–178.

[23] R. Shams, M.-A. Boucher, and S. Kadoury, "Intra-operative brain shift correction with weighted locally linear correlations of 3DUS and MRI," in *Simulation, Image Processing, and Ultrasound Systems for Assisted Diagnosis and Navigation* (Lecture Notes in Computer Science). Springer, 2018, ch. 22, pp. 179–184.

[24] W. Wein, A. Ladikos, B. Fuerst, A. Shah, K. Sharma, and N. Navab, "Global registration of ultrasound to MRI using the LC² metric for enabling neurosurgical guidance," in *Medical Image Computing and Computer-Assisted Intervention*. Berlin, Germany: Springer, 2013, pp. 34–41.

[25] M. P. Heinrich, M. Jenkinson, B. W. Papież, S. M. Brady, and J. A. Schnabel, "Towards realtime multimodal fusion for image-guided interventions using self-similarities," in *Medical Image Computing and Computer-Assisted Intervention*. Berlin, Germany: Springer, 2013, pp. 187–194.

[26] V. A. Zimmer, M. Á. G. Ballester, and G. Piella, "Multimodal image registration using Laplacian commutators," *Inf. Fusion*, vol. 49, pp. 130–145, Sep. 2019, doi: 10.1016/j.inffus.2018.09.009.

[27] I. Machado, M. Toews, E. George, P. Unadkat, W. Essayed, J. Luo, P. Teodoro, H. Carvalho, J. Martins, P. Golland, S. Pieper, S. Frisken, A. Golby, W. Wells, III, and Y. Ou, "Deformable MRI-ultrasound registration using correlation-based attribute matching for brain shift correction: Accuracy and generality in multi-site data," *NeuroImage*, vol. 202, Nov. 2019, Art. no. 116094, doi: 10.1016/j.neuroimage.2019.116094.

[28] A. Krizhevsky, I. Sutskever, and G. E. Hinton, "ImageNet classification with deep convolutional neural networks," *Commun. ACM*, vol. 60, no. 6, pp. 84–90, 2017, doi: 10.1145/3065386.

[29] K. He, X. Zhang, S. Ren, and J. Sun, "Deep residual learning for image recognition," in *Proc. IEEE Conf. Comput. Vis. Pattern Recognit. (CVPR)*, Jun. 2016, pp. 770–778.

[30] O. Ronneberger, P. Fischer, and T. Brox, "U-Net: Convolutional networks for biomedical image segmentation," in *Medical Image Computing and Computer-Assisted Intervention—MICCAI* (Lecture Notes in Computer Science). Springer, 2015, ch. 28, pp. 234–241.

[31] R. A. Zeineldin, M. E. Karar, J. Coburger, C. R. Wirtz, and O. Burgert, "DeepSeg: Deep neural network framework for automatic brain tumor segmentation using magnetic resonance FLAIR images," *Int. J. Comput. Assist. Radiol. Surg.*, vol. 15, no. 6, pp. 909–920, Jun. 2020, doi: 10.1007/s11548-020-02186-z.

[32] K. Saleh, R. A. Zeineldin, M. Hossny, S. Nahavandi, and N. El-Fishawy, "End-to-end indoor navigation assistance for the visually impaired using monocular camera," in *Proc. IEEE Int. Conf. Syst., Man, Cybern. (SMC)*, Oct. 2018, pp. 3504–3510.

[33] K. Armanious, C. Jiang, M. Fischer, T. Küstner, T. Hepp, K. Nikolaou, S. Gatidis, and B. Yang, "MedGAN: Medical image translation using GANs," *Comput. Med. Imag. Graph.*, vol. 79, Jan. 2020, Art. no. 101684, doi: 10.1016/j.compmedimag.2019.101684.

[34] J. Dolz, C. Desrosiers, L. Wang, J. Yuan, D. Shen, and I. B. Ayed, "Deep CNN ensembles and suggestive annotations for infant brain MRI segmentation," *Comput. Med. Imag. Graph.*, vol. 79, Jan. 2020, Art. no. 101660, doi: 10.1016/j.compmedimag.2019.101660.

[35] Y. LeCun, Y. Bengio, and G. Hinton, "Deep learning," *Nature*, vol. 521, no. 7553, pp. 436–444, 2015, doi: 10.1038/nature14539.

[36] M.-M. Rohé, M. Datar, T. Heimann, M. Sermesant, and X. Pennec, "SVF-Net: Learning deformable image registration using shape matching," in *Medical Image Computing and Computer Assisted Intervention—MICCAI*. Cham, Switzerland: Springer, 2017, pp. 266–274.

[37] X. Cheng, L. Zhang, and Y. Zheng, "Deep similarity learning for multimodal medical images," *Comput. Methods Biomech. Biomed. Eng., Imag. Vis.*, vol. 6, no. 3, pp. 248–252, May 2018, doi: 10.1080/21681163.2015.1135299.

[38] K. Ma, J. Wang, V. Singh, B. Tamersoy, Y.-J. Chang, A. Wimmer, and T. Chen, "Multimodal image registration with deep context reinforcement learning," in *Medical Image Computing and Computer Assisted Intervention—MICCAI*. Cham, Switzerland: Springer, 2017, pp. 240–248.

[39] X. Yang, R. Kwitt, M. Styner, and M. Niethammer, "Quicksilver: Fast predictive image registration—A deep learning approach," *NeuroImage*, vol. 158, pp. 378–396, Sep. 2017, doi: 10.1016/j.neuroimage.2017.07.008.

[40] Y. Hu, M. Modat, E. Gibson, W. Li, N. Ghavami, E. Bonmati, G. Wang, S. Bandula, C. M. Moore, M. Emberton, and S. Ourselin, "Weakly-supervised convolutional neural networks for multimodal image registration," *Med. Image Anal.*, vol. 49, pp. 1–13, Oct. 2018, doi: 10.1016/j.media.2018.07.002.

[41] J. Lee, P. Liu, J. Cheng, and H. Fu, "A deep step pattern representation for multimodal retinal image registration," in *Proc. IEEE/CVF Int. Conf. Comput. Vis. (ICCV)*, Oct. 2019, pp. 5077–5086.

[42] G. Haskins, J. Kruecker, U. Kruger, S. Xu, P. A. Pinto, B. J. Wood, and P. Yan, "Learning deep similarity metric for 3D MR–TRUS image registration," *Int. J. Comput. Assist. Radiol. Surg.*, vol. 14, no. 3, pp. 417–425, Mar. 2019, doi: 10.1007/s11548-018-1875-7.

[43] H. Li and Y. Fan, "Non-rigid image registration using self-supervised fully convolutional networks without training data," in *Proc. IEEE 15th Int. Symp. Biomed. Imag. (ISBI)*, Apr. 2018, pp. 1075–1078, doi: 10.1109/ISBI.2018.8363757.

[44] G. Balakrishnan, A. Zhao, M. R. Sabuncu, J. Guttag, and A. V. Dalca, "VoxelMorph: A learning framework for deformable medical image registration," *IEEE Trans. Med. Imag.*, vol. 38, no. 8, pp. 1788–1800, Aug. 2019, doi: 10.1109/TMI.2019.2897538.

[45] B. D. de Vos, F. F. Berendsen, M. A. Viergever, H. Sokooti, M. Staring, and I. Išgum, "A deep learning framework for unsupervised affine and deformable image registration," *Med. Image Anal.*, vol. 52, pp. 128–143, Feb. 2019, doi: 10.1016/j.media.2018.11.010.

[46] Y. Xiao, H. Rivaz, M. Chabanas, M. Fortin, I. Machado, Y. Ou, M. P. Heinrich, J. A. Schnabel, X. Zhong, A. Maier, W. Wein, R. Shams, S. Kadoury, D. Drobny, M. Modat, and I. Reinertsen, "Evaluation of MRI to ultrasound registration methods for brain shift correction: The CuRIOUS2018 challenge," *IEEE Trans. Med. Imag.*, vol. 39, no. 3, pp. 777–786, Mar. 2020, doi: 10.1109/TMI.2019.2935060.

[47] X. Zhong, S. Bayer, N. Ravikumar, N. Strobel, A. Birkhold, M. Kowarschik, R. Fahrig, and A. Maier, "Resolve intraoperative brain shift as imitation game," in *Simulation, Image Processing, and Ultrasound Systems for Assisted Diagnosis and Navigation* (Lecture Notes in Computer Science). Springer, 2018, ch. 15, pp. 129–137.

[48] L. Sun and S. Zhang, "Deformable MRI-ultrasound registration using 3D convolutional neural network," in *Simulation, Image Processing, and Ultrasound Systems for Assisted Diagnosis and Navigation* (Lecture Notes in Computer Science). Springer, 2018, ch. 18, pp. 152–158.

[49] R. A. Zeineldin, M. E. Karar, J. Coburger, C. R. Wirtz, F. Mathis-Ullrich, and O. Burgert, "Towards automated correction of brain shift using deep deformable magnetic resonance imaging-intraoperative ultrasound (MRI-iUS) registration," *Current Directions Biomed. Eng.*, vol. 6, no. 1, Sep. 2020, Art. no. 20200039, doi: 10.1515/cdbme-2020-0039.

[50] K. Kneöaurek, M. Ivanovic, J. Machac, and D. A. Weber, "Medical image registration," *Europhys. News*, vol. 31, no. 4, pp. 5–8, Jul. 2000, doi: 10.1051/epn:2000401.

[51] M. E. Karar, D. R. Merk, V. Falk, and O. Burgert, "A simple and accurate method for computer-aided transapical aortic valve replacement," *Comput. Med. Imag. Graph.*, vol. 50, pp. 31–41, Jun. 2016, doi: 10.1016/j.compmedimag.2014.09.005.

[52] Ö. Çiçek, A. Abdulkadir, S. S. Lienkamp, T. Brox, and O. Ronneberger, "3D U-Net: Learning dense volumetric segmentation from sparse annotation," in *Medical Image Computing and Computer-Assisted Intervention—MICCAI* (Lecture Notes in Computer Science). Springer, 2016, ch. 49, pp. 424–432.

[53] X. Glorot and Y. Bengio, "Understanding the difficulty of training deep feedforward neural networks," presented at the 13th Int. Conf. Artif. Intell. Statist., 2010. [Online]. Available: https://proceedings.mlr.press/v9/glorot10a.html

[54] C. Sammut and G. I. Webb, Eds., "Mean squared error," in *Encyclopedia of Machine Learning*. Boston, MA, USA: Springer, 2010, p. 653.

[55] A. Roche, G. Malandain, N. Ayache, and S. Prima, "Towards a better comprehension of similarity measures used in medical image registration," in *Medical Image Computing and Computer-Assisted Intervention—MICCAI*. Berlin, Germany: Springer, 1999, pp. 555–566.

[56] L. Mercier, R. F. Del Maestro, K. Petrecca, D. Araujo, C. Haegelen, and D. L. Collins, "Online database of clinical MR and ultrasound images of brain tumors," *Med. Phys.*, vol. 39, no. 6, pp. 3253–3261, Jun. 2012, doi: 10.1118/1.4709600.

[57] Y. Xiao, M. Fortin, G. Unsgard, H. Rivaz, and I. Reinertsen, "REtro-Spective evaluation of cerebral tumors (RESECT): A clinical database of pre-operative MRI and intra-operative ultrasound in low-grade glioma surgeries," *Med. Phys.*, vol. 44, no. 7, pp. 3875–3882, Jul. 2017, doi: 10.1002/mp.12268.

[58] R. D. Vincent, P. Neelin, N. Khalili-Mahani, A. L. Janke, V. S. Fonov, S. M. Robbins, L. Baghdadi, J. Lerch, J. G. Sled, R. Adalat, D. MacDonald, A. P. Zijdenbos, D. L. Collins, and A. C. Evans, "MINC 2.0: A flexible format for multi-modal images," *Frontiers Neuroinform.*, vol. 10, p. 35, Aug. 2016, doi: 10.3389/fninf.2016.00035.

[59] L. Mercier, V. Fonov, C. Haegelen, R. F. Del Maestro, K. Petrecca, and D. L. Collins, "Comparing two approaches to rigid registration of three-dimensional ultrasound and magnetic resonance images for neurosurgery," *Int. J. Comput. Assist. Radiol. Surg.*, vol. 7, no. 1, pp. 125–136, Jan. 2012, doi: 10.1007/s11548-011-0620-2.

[60] J. Hong and H. Park, "Non-linear approach for MRI to intra-operative U.S. Registration using structural skeleton," in *Simulation, Image Processing, and Ultrasound Systems for Assisted Diagnosis and Navigation* (Lecture Notes in Computer Science). Springer, 2018, ch. 16, pp. 138–145.

RAMY A. ZEINELDIN (Member, IEEE) received the B.S. (Hons.) and M.S. degrees in computer science and engineering from the Faculty of Electronic Engineering, Menoufia University, Egypt, in 2013 and 2018, respectively. He is currently pursuing the Ph.D. degree in medical engineering with the Health Robotics and Automation Laboratory, Karlsruhe Institute of Technology (KIT), Germany.

From 2013 to 2018, he was a Teaching Assistant with the Department of Computer Science and Engineering, Faculty of Electronic Engineering, Menoufia University. Since 2019, he has been a Research Assistant with the Research Group Computer Assisted Medicine (CaMed), Reutlingen University, Germany. His research interests include artificial intelligence, machine learning, computer vision, medical engineering, and robotics.

Mr. Zeineldin awards and honors include the Idea to Product (I2P) Global Competition at Sao Paulo, Brazil, in 2013, the German Academic Exchange Service (DAAD) Fellowship, in 2018, chosen as One of the Young Researchers in Heidelberg Laureate Forum, in 2020 and 2021, and the Best Poster Award from the German Society for Computer- and Robot-Assisted Surgery (CURAC), in 2020.

MOHAMED E. KARAR (Member, IEEE) received the B.Sc. (Hons.) and M.Sc. degrees in electronic engineering from the Faculty of Electronic Engineering, Menoufia University, in 2000 and 2006, respectively, and the Dr.Eng. degree in computer assisted surgery from the University of Leipzig, Germany, in 2012, based on the German Exchange Service (DAAD) Fellowship.

In 2015, he received the German Egyptian Short-Term Scholarship (GERSS) as a Postdoctoral Fellow in the field of medical robotics at the Technical University of Munich (TUM), Germany. From 2018 to 2019, he was the Head of the Department of Industrial Electronics and Control Engineering, Menoufia University. Since March 2019, he has been a Visiting Professor at the College of Computing and Information Technology, Shaqra University, Saudi Arabia.

Dr. Karar won the prize of a Distinguished Faculty Member Award from Menoufia University, in 2016. He published many papers in various reputed international journals and conferences in the field of intelligent systems and control. His main research interests include medical image, signal processing, and intelligent systems.

ZIAD ELSHAER received the B.S. degree in medicine and surgery and the M.S. degree in neurosurgery from Ain Shams University, Egypt, in 2010 and 2013, respectively.

From 2012 to 2016, he attended the Neurosurgical Residency Program at Ain Shams University Hospitals, Egypt. He is currently a Specialist with the Department of Neurosurgical Surgery, Ulm University Medical Center, Ulm, Germany. His main research interests include neuro-oncology, neuroanatomy, and intraoperative imaging.

MARKUS SCHMIDHAMMER is a resident at the Department of Neurosurgery, Ulm University Hospital, Germany. His main research interests include neuro-oncology, neuroanatomy, and intraoperative imaging.

JAN COBURGER has been a Consultant at the Department of Neurosurgery, Ulm University Hospital, Germany, since 2012. He has published many papers in various reputed international journals and conferences in the field of neurosurgery and intraoperative imaging. His main research interests include neuro-oncology, neuroendoscopy, and intraoperative imaging.

He won the Best International Abstract Award from the American Association of Neurological Surgeons (AANS), in 2014.

CHRISTIAN R. WIRTZ has been the Head of the Department of Neurosurgery, Ulm University Hospital, Germany, since 2008.

OLIVER BURGERT received the Dr.Eng. degree in volume-based surgical simulation and planning from the University of Karlsruhe, Germany, in 2005.

From 2005 to 2011, he was the Scientific Director of the Innovation Centre Computer Assisted Surgery (ICCAS), Research Group, University of Leipzig, Germany. Since October 2011, he has been a Professor of medical informatics at Reutlingen University. He is currently the Dean of the Faculty of Informatics and the Head of the Research Group Computer Assisted Medicine, Reutlingen University. He has experience in standardization. He was responsible for several DICOM supplements. He is interested in modern teaching methods and teaches foundational courses in computer science as well as advanced topics in informatics applications in medicine. His research interests include intelligent operating room and optimization of the perioperative area.

Prof. Burgert was among the first people receiving the "Baden-Württemberg-Zertifikat Hochschuldidaktik," participated in the first and second edition of the accreditation guidelines for the bachelor's degree in computer science from the German Informatics Society, a Board Member of the German Society for Computer and Robotic-Assisted Surgery (CURAC), a member of several other scientific organizations and numerous program committees of conferences in the field of computer-assisted medicine, an Editorial Board Member of the *International Journal of Computer Assisted Radiology and Surgery*, and a reviewer of several other journals.

FRANZISKA MATHIS-ULLRICH received the B.Sc. and M.Sc. degrees in mechanical engineering and robotics and the Ph.D. degree in microrobotics from ETH Zurich, in 2009, 2012, and 2017, respectively.

Since 2019, she has been an Assistant Professor with the Health Robotics and Automation Laboratory, Karlsruhe Institute of Technology (KIT), Germany, where she is currently an Assistant Professor of medical robotics. She is also the Vice President of the German Society for Computer- and Robot-Assisted Surgery (CURAC). Her primary research interests include minimally invasive and cognition controlled robotic systems and embedded machine learning with emphasis on applications in surgery. She received the IEEE ICRA Best Paper Award in medical robotics, in 2014, the IEEE BioRob Best Student Paper Award, in 2016, and won twice with her team the first prize of the ICRA Microassembly Challenge, in 2014 and 2015. She also made it onto the prestigious Forbes "30 under 30" list, in 2017.

· · ·